https://doi.org/10.5194/tc-2022-258
Preprint. Discussion started: 22 February 2023

The Cryosphere Discussions
Open Access
EGU

Title: Black carbon concentrations and modeled smoke deposition fluxes to the bare ice dark zone of the Greenland Ice Sheet

Authors: Alia L. Khan[1], Peng Xian[2], Joshua Schwarz[3]

[1]Department of Environmental Sciences, Western Washington University

[2]Aerosol and Radiation Section of the Marine Meteorology Division, Naval Research Laboratory, Monterey, California, USA

[3]Chemical Sciences Division, NOAA Earth System Research Laboratory (ESRL), Boulder, CO, United States

***Correspondence to*:** Alia L. Khan (alia.khan@wwu.edu)

Abstract:

Ice-albedo feedbacks in the ablation region of the Greenland Ice Sheet (GrIS) are difficult to constrain and model due in part to our limited understanding of the seasonal evolution of the bare-ice region. To help fill observational gaps, 13 surface samples were collected on the GrIS across the 2014 summer melt season from patches of snow that were visibly light, medium, and dark colored. These samples were analyzed for their refractory black carbon (rBC) concentrations and size distributions with a Single Particle Soot Photometer coupled to a characterized nebulizer. We present a size distribution of rBC in fresh snow on the GrIS, as well as from surface hoar in the bare ice dark zone of the GrIS. The size distributions from the surface hoar samples appear unimodal, and were overall smaller than the fresh snow sample, with a peak around 0.3 µm. The fresh snow sample contained very large rBC particles that had a pronounced bimodality in peak size distributions, with peaks around 0.2 µm and 2 µm. rBC concentrations ranged from a minimum of 3 µg-rBC/L-H_2O in light-colored patches at the beginning and end of the melt season, to a maximum of 32 µg-rBC/L-H_2O in a dark patch in early August. On average, rBC concentrations were higher (20 µg-rBC/L-H_2O ± 10 µg-rBC/L-

https://doi.org/10.5194/tc-2022-258
Preprint. Discussion started: 22 February 2023


The Cryosphere Discussions

H_2O) in patches that were visibly dark compared to medium patches (7 µg-rBC/L-H_2O ± 2 µg-rBC/L-H_2O) and light patches (4 µg-rBC/L-H_2O ± 1 µg-rBC/L-H_2O), suggesting BC aggregation contributed to snow aging on the GrIS, and vice versa. Additionally, concentrations peaked in light and dark patches in early August, which is likely due to smoke transport from wildfires in Northern Canada and Alaska as supported by the Navy Aerosol Analysis and Prediction System (NAAPS) reanalysis model. According to model output, 26 mg/m^3 of biomass burning derived smoke was deposited between April 1st and August 30th, of which 85% came from wet deposition and 67% was deposited during our sample collection timeframe. The increase in rBC concentration and size distributions immediately after modelled smoke deposition fluxes suggest biomass burning smoke is a source of BC to the dark zone of the GRIS. Thus, role of BC in the seasonal evolution of the ice-albedo feedback should continue to be investigated in the bare-ice zone of the GrIS.

1. Introduction

The bare ice dark zone of the southwest Greenland Ice Sheet (GrIS) is characterized by low albedo due in part to the presence of light absorbing impurities (LAIs), that create a positive ice-albedo feedback through increased surface melting, ice grain growth, and darkening (Tedesco et al., 2016). LAIs in this region are a mixture of cryoconite, ice algae (Stibal et al., 2017; Ryan et al., 2018), dust (Wientjes et al., 2011), and black carbon (BC) such as from Northern Hemisphere fires (Khan et al., 2017), yet the relative contribution of each light absorbing particle is still uncertain. The radiative forcing of these LAIs, along with warming summer surface temperatures (Hanna et al., 2008), leads to large volumes of supra-glacial melt (Greuell, 2000).

https://doi.org/10.5194/tc-2022-258
Preprint. Discussion started: 22 February 2023

Furthermore, retreat of the snowline is amplifying surface melt of the GrIS due to increased bare ice exposure (Ryan et al., 2019) and the LAI-ice albedo feedbacks described above.

BC in and on snow and ice is known to warm the Arctic and contribute to snow and ice melting, however the magnitude of its influence is still highly uncertain e.g., (Flanner et al., 2007; Bond et al., 2013). BC concentration in air is typically operationally defined depending on the analytical technique used (Petzold et al., 2013). Many in-situ measurements of BC concentration in snow in the Arctic have been reported by the Integrating Plate and Integrating Sandwich (IS) technique, which provides analysis of light absorption of particulate impurities through spectrophotometric analysis of filter loaded with particulates collected from melted samples (e.g., Clarke and Noone, 1985; Doherty et al., 2010; Doherty et al., 2013). Doherty et al. (2010) reported a median concentration of 3 ng/g in surface snow, with higher concentrations layers up to ~20ng/g in snow profiles at Dye 2. Snow samples from snowpits in the northwest sector of the GrIS were also collected in 2013 and 2014 from two traverses and analyzed for elemental/organic carbon (EC/OC) and was determined to not influence the snow albedo in this region with a mean of 2.6 ng/g and a mean peak of 15 ng/g (Polashenski et al., 2015a). Observations of refractory black carbon (rBC) analyzed by the Single Particle Soot Photometer (SP2) have been published from snow profiles and ice cores in the accumulation region closer to the Summit research station (McConnell et al., 2007a; Keegan et al., 2014b; Lim et al., 2014). McConnell et al. (2007) presented BC concentrations from a 215-year ice-core record collected at D4 in West Central Greenland with average concentrations of 1.7ng/g in pre-industrial times, 2.3ng/g over the period 1950-2002, and around 5 ng/g in the peak period of the early 1900s. The maximum monthly concentration observed was 58.8 ng/g in 1854, however, monthly concentrations only exceeded 5 ng/g ~2-3 times each decade after 1950. Polashenski et al.,

https://doi.org/10.5194/tc-2022-258
Preprint. Discussion started: 22 February 2023

(2015) provides a comprehensive review of previous BC concentrations in their supplemental info, showing that the BC average ranges between 1.5 and 3 ng/g over an annual cycle, with peak deposition occurring during summer episodic events, with concentrations of 5 - 10+ ng/g only occurring a few times at a given site per decade.

rBC measured by SP2 has been shown to provide more reliable measurements of concentration than the IS or EC/OC (from liquid and air samples, respectively) techniques because it is largely free from the interference of materials other than rBC (Kondo et al., 2011; Schwarz et al., 2012) such as pyrolyzed organic carbon artifacts (Lim et al., 2014). It also provides a lower detection limit and increased sensitivity at low concentrations (Lim et al. 2014). The SP2 coupled with a nebulizer also provides a measurement of rBC particle size distribution from liquid samples.

rBC particle size has been observed in some snow samples to be larger than expected from atmospheric measurements, reflecting to some degree size-dependent removal processes from the atmosphere (Schwarz et al., 2013). The rBC size distribution in snow, which at this point is constrained by direct observations not supported by detailed modeling, is a significant source of uncertainty for calculating the overall radiative forcing of BC-in-snow on the Arctic climate, as well as the global climate (e.g., Bond et al., 2013). Very few rBC size distributions in snow have been reported globally, with most measurements coming from the Arctic (Lim et al., 2014; Khan et al., 2017; Mori et al., 2019).

Although, observations of BC in snow have been previously observed in the percolation zone (Dye 2) and accumulation zone (Summit Station) by the IS technique (Doherty et al., 2010a, 2013) and rBC-SP2 at Summit Station (McConnell et al., 2007b; Keegan et al., 2014a; Lim et al., 2014), to the authors' knowledge, no reports of rBC concentrations with size distributions in snow and

https://doi.org/10.5194/tc-2022-258
Preprint. Discussion started: 22 February 2023

surface hoar have been reported from the GrIS, providing new insight, particularly into the dynamic bare-ice region.

Here we present rBC concentrations with size distributions from the bare ice region of the GrIS before and after influence by a major wildfire event, along with NAAPS modelled wet and dry deposition. Our findings suggests that rBC surface hoar concentrations in the bare ice zone reflect atmospheric conditions momentarily, before being reset, possibly by supra-glacial melt. Additionally, NAAPS model output suggest most of the biomass burning derived smoke deposition comes in the form of wet removal (i.e., removal by precipitation). These rBC concentrations and size distributions provide insight into the seasonal evolution of impurities, which are needed to constrain ice-albedo feedbacks in the bare-ice zone of the GrIS.

2. Methods

2.1 Site Description and Snow Sampling

The field site was in the southwestern region of the GrIS near the S6 automated weather station at 67 04.779'N, 49 24.077'W, and 1011 m above sea level. More information on the study site can be found in Stibal et al. (2017). A fresh snow surface sample (2 – 3 cm), was collected just after a snow event on 2014-06-27. Three surface hoar samples (2 – 3 cm), were collected in pre-cleaned and combusted amber glass bottles four times between 2014-06-28 and 2014-08-11 across the 2014 summer melt season from visually identified light, medium, and dark patches of surface hoar, for a total of 13 samples, including the fresh snow. While all sample sites could include a mixture of ice algae, dust, black carbon (i.e, cryoconite), the dark patches especially could represent refrozen melt that is enhanced in LAIs, including rBC. A mixture of light, medium and dark 1 – 3 m^2 patches were sampled within the ~.5 km^2 study area to characterize

https://doi.org/10.5194/tc-2022-258
Preprint. Discussion started: 22 February 2023

119 the breadth of surface types and heterogenous distribution of impurities. Samples were stored
120 frozen in a 'field cooler' dug into the ice and then transported frozen on ice to Kangerlussuaq,
121 and shipped on dry ice to the Denver Airport, and then transported immediately to a freezer at
122 the Institute of Arctic and Alpine Research (INSTAAR) at the University of Colorado – Boulder.

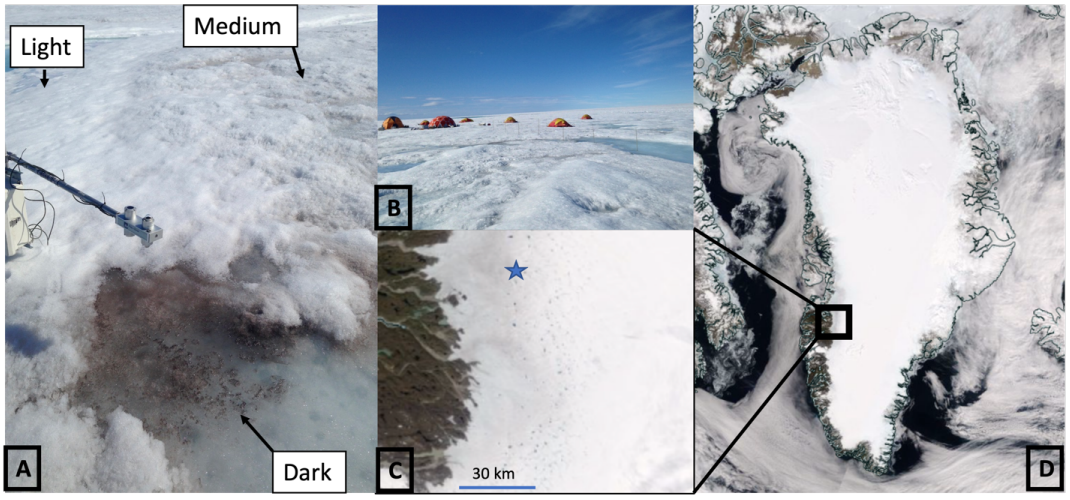

123 A and B are images collected by Dr. Alia Khan. C and D are MODIS satellite images acquired from the NASA Worldview application.

124 **Figure 1:** A) Example light, medium and dark patches of ice. B) The Dark Snow Field Camp. C)
125 The southwest GrIS dark zone with the field sampling location indicated by a blue star and D)
126 the GrIS from MODIS on July 2nd, 2014. A and B are photos collected by Alia Khan. C and D
127 are MODIS satellite images acquired from the NASA Worldview application
128 (https://worldview.earthdata.nasa.gov/), part of the NASA Earth Observing System Data and
129 Information System (EOSDIS).

130

131 *2.2 Processing for Refractory Black Carbon*

132 The samples were transported frozen from INSTAAR to the Earth System Research Laboratory
133 at the National Oceanic and Atmospheric Administration where they were analyzed for rBC
134 mass mixing ratios (MMRs) by SP2 coupled to a nebulizer per the methods described in Katich

https://doi.org/10.5194/tc-2022-258
Preprint. Discussion started: 22 February 2023

et al. (2017) and Khan et al. (2018). Briefly, the samples were melted for the first time just prior to analysis with the SP2 and aerosolized with a carefully calibrated concentric pneumatic nebulizer based on a customized U5000 AT+ nebulizer (Teledyne Cetac, Inc.) which the ultrasonic piezo was replaced with a concentric pneumatic nebulizer. The SP2 was calibrated with fullerene soot (Lot# F12S011, Alfa Aesar Inc., Wood Hill, MA) with the community calibration approach (Baumgardner et al., 2012) over masses of 1 – 20 fg. Using a power law calibration dependence following Schwarz et al., [2012], the resulting linear calibration of SP2 signal to rBC mass applied to mass of 80 fg was extended further to 4000 fg. The SP2 was operated with a widely staggered gain for two incandescent channels, allowing sizing of rBC mass in the range ~1 – 4000 fg.

Melted snow samples were interspersed with deionized water blanks to confirm a low background, especially relative to the MMRs, indicating no appreciable contamination to concentrations and size distributions. Little size-dependence in nebulization efficiency was confirmed with concentration standards of polystyrene latex spheres (PSLs) over 220 – 1500 nm diameter, which is consistent with recent results from concentric pneumatic nebulizers (Wendl et al., 2014, Katich et al., 2017). Therefore, size dependent corrections were not necessary. During data acquisition with the SP2, its lower mass-detection limit was 1.2 fg, which corresponds to about a 110 nm volume equivalent diameter (VED) size detection limit, assuming 1.8g/cc void free density. A 510 nm diameter PSL concentration standard was sampled between melted snow analyses to track possible changes in nebulization efficiency during each day of sampling. This revealed effectively constant efficiency varying with a standard deviation less than 5%. A gravimetric mass concentration standard (Schwarz et al., 2012) was also used to evaluate nebulization efficiency. The results of the PSL and gravimetric calibrations of nebulizer

https://doi.org/10.5194/tc-2022-258
Preprint. Discussion started: 22 February 2023

158 efficiency were consistent within uncertainties of 20% and were averaged to provide a best-
159 estimate nebulization efficiency that was then used to produce the BC MMR values as in
160 Schwarz et al. (2012).
161
162 2.3 *Global Aerosol Modeling*
163 The Navy Aerosol Analysis Prediction System (NAAPS) model is a global aerosol transport
164 model which provides 6-hrly biomass burning smoke, anthropogenic and biogenic fine aerosols,
165 dust, and sea salt aerosol forecasts and analyses below 100 hPa at 1/3° latitude/longitude spatial
166 resolution and contains 42 vertical atmospheric levels. The NAAPS reanalysis (NAAPS-RA) is
167 available 2003-current with a coarser spatial resolution (1° latitude/longitude horizontal and 25
168 vertical levels) (Lynch et al., 2016). Total column aerosol optical thickness (AOT) is constrained
169 through assimilation of quality-controlled satellite AOT retrievals from the Moderate Imaging
170 Spectroradiometer (MODIS) and Multi-angle Imaging SpectroRadiometer (MISR). Near-real
171 time satellite based thermal anomaly data enables detection of wildfires and construction of
172 biomass burning smoke emissions (Reid et. al., 2009). Orbital corrections for MODIS-based fire
173 detections and regional factors were applied on emissions so that the reanalysis AOT verifies
174 well with ground-based measurements (Lynch et al., 2016). The NAAPS-RA has been applied to
175 a broad range of science applications, and specifically the life cycle, climatology, radiative
176 forcing, aerosol-atmosphere-ice-ocean interactions of biomass burning smoke aerosols (e.g.,
177 Reid et al., 2012; Xian et al., 2013; Markowicz et al., 2021; Ross et al., 2018; Khan et al., 2019;
178 Carson-Marquis et al., 2021), as well as previously to corroborate wildfire smoke transport to the
179 GrIS (Khan et al., 2017), Arctic Canada (Ranjbar et al., 2019), Svalbard (Markowicz et al., 2016;
180 2017), the pan-Arctic region (Xian et al., 2022a, b), the Nepalese Himalayas (Khan et al., 2020),

https://doi.org/10.5194/tc-2022-258
Preprint. Discussion started: 22 February 2023

and the Antarctic (Khan et al., 2018; Khan et al., 2019). Speciated AOT, surface aerosol concentration and deposition flux are used in this study. Here the deposition is calculated as 24-hour flux to the surface of the ice sheet in mg/m^2/day. The mass ratio of rBC to total mass in biomass burning smoke particles is assumed to be 7%, which is an approximate median value from literatures (i.e., Reid et al., 2005)

3. Results and Discussion

3.1 rBC Concentrations

rBC concentrations in the surface hoar ranged from a minimum of 3 µg-rBC/L-H_2O in light patches at the beginning and end of the melt season, to a peak of 32 µg-rBC/L-H_2O in a dark patch in early August (Table 1). rBC concentrations were higher in patches that were visibly darker (20 µg-rBC/L-H_2O) compared to medium patches (7 µg-rBC/L-H_2O) and light patches (4 µg-rBC/L-H_2O), suggesting BC aggregates with dust and biological material on the GrIS. Light and dark patch concentrations peaked in early August. Our minimum concentrations are in the range of rBC concentrations found elsewhere on the GrIS, but our peaks are higher than previously reported concentrations from snow on the GrIS (Doherty et al., 2010a; Polashenski et al., 2015). Our maximum concentrations are higher than the highest concentrations observed in vertical snow with the IS (Doherty et al., 2010b) and EC/OC technique (Polashenski et al., 2015), but less than the highest monthly average concentration of year of 1854 reported in an ice core by McConnell et al. (2007). The concentration of rBC in the fresh snow (3 µg-rBC/L-H_2O) sample was roughly the same as the light surface hoar patches on 2014-06-28 and 2014-08-11.

Table 1: NAAPs Smoke Dry, Wet, and Total Deposition (mg/m^2/day) from April 1st prior to sample collection. Average rBC concentrations from visually light, medium, and dark patches of

https://doi.org/10.5194/tc-2022-258
Preprint. Discussion started: 22 February 2023

surface hoar. All samples were collected at 67.07979701 degrees N and -49.40116603 degrees W at 1005 meters above sea level in the dark zone ablation region of the SW Greenland Ice Sheet.

^The fresh snow sample is a single sample.

Date	NAAPS Smoke Dry Deposition (mg/m³/day)	NAAPs Smoke Wet Deposition (mg/m³/day)	NAAPs Smoke Total Deposition (mg/m²/day)	Average rBC μg-rBC/L-H_2O	Snow type (visual color)	rBC μg-rBC/L-H_2O
6/27/14	0.58	1.98	2.56	3.05^	Fresh	3.05
6/28/14	0.60	6.92	7.51	8.37	Light	2.87
					Medium	9.61
					Dark	12.62
7/21/14	0.75	6.93	7.69	11.45	Light	4.21
					Medium	6.42
					Dark	23.71
8/2/14	1.51	9.44	10.95	14.15	Light	5.27
					Medium	4.71
					Dark	32.47
8/11/14	1.94	12.14	14.08	8.12	Light	2.96
					Medium	8.75
					Dark	12.64

3.2 rBC Size Distributions

We found very large rBC are present (Figure 2A and B), especially in the fresh snow sample. The large sizes distribution in fresh snow follows previous findings in the rocky mountains that rBC size distributions can be larger in surface snow than expected in aerosol in the atmosphere (Schwarz et al., 2013). Furthermore, the fresh event is associated with a more pronounced

https://doi.org/10.5194/tc-2022-258
Preprint. Discussion started: 22 February 2023

bimodality at ~ 0.2 µm and 2 µm (Figure 2A), whereas the rBC in surface hoar samples appears more unimodal (Figure 2B). The average surface hoar rBC sizes, which have not been previously reported in the literature, are smaller than the one fresh snow sample with a peak around 0.3 µm. This is still larger than typical modal sizes for rBC observed in the atmosphere (in the range ~0.11 – 0.2 µm typically). Furthermore, no apparent patterns emerge in the size distributions across the light, medium and dark patches over the duration of the season. However, the surface hoar rBC size distributions likely evolve, just as the seasonal snow cover evolves into bare ice and surface hoar, but we are unable to assess from this relatively small data set. This conjecture is supported by observations that repeated freeze/thaw cycles tend to cause rBC coagulation in liquid (Schwarz et al., 2013). Regardless, these initial results of rBC size distributions from fresh snow and surface hoar in the bare ice region of the GrIS are important for informing ice-albedo models, which are still being developed and refined for bare ice regions of the ice sheet (e.g. Flanner et al., 2007).

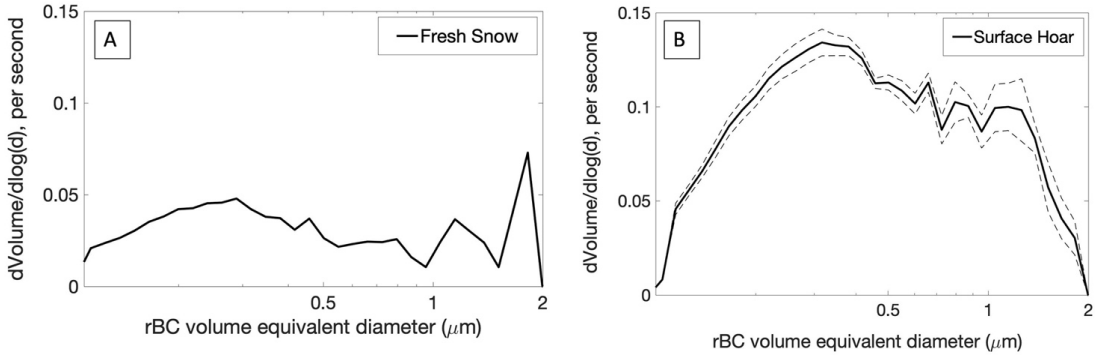

Figure 2: A) rBC size distribution of fresh snow (n=1) and B) all surface hoar samples over the duration of the season (n=12). The dashed lines in Figure 2B represent the max and min size distributions and the solid black line is the average.

https://doi.org/10.5194/tc-2022-258
Preprint. Discussion started: 22 February 2023

231 *3.3 NAAPS Aerosol Model Comparison and Evaluation*

232 The ground observations were then compared to cumulative aggregates of smoke deposition
233 fluxes modelled with the Navy Aerosol Analysis Prediction System reanalysis model. AOT
234 derived from MODIS and modeled by NAAPS demonstrates that a large wildfire smoke event
235 was observed just before the third sample was collected and during the time the fourth sample
236 was collected (Figure 3). Concomitant AOT and surface concentration predictions from the
237 NAAPS model confirms our peak concentrations are likely due to Northern Hemisphere wildfire
238 smoke (Figure 4 A- D).

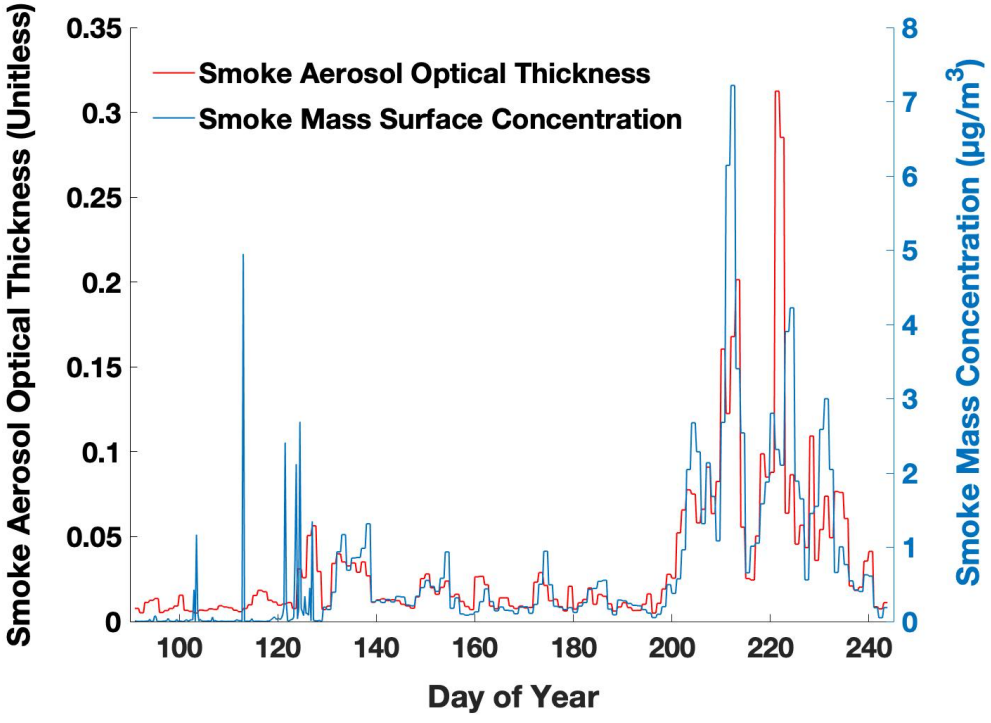

239

240 **Figure 3:** Aerosol optical thickness (AOT) derived from NAAPS reanalysis

https://doi.org/10.5194/tc-2022-258
Preprint. Discussion started: 22 February 2023

241 over the sampling season from smoke and dust. B) Smoke mass concentration (µg/m^3) in the
242 surface layer of the model (centered around 16m).

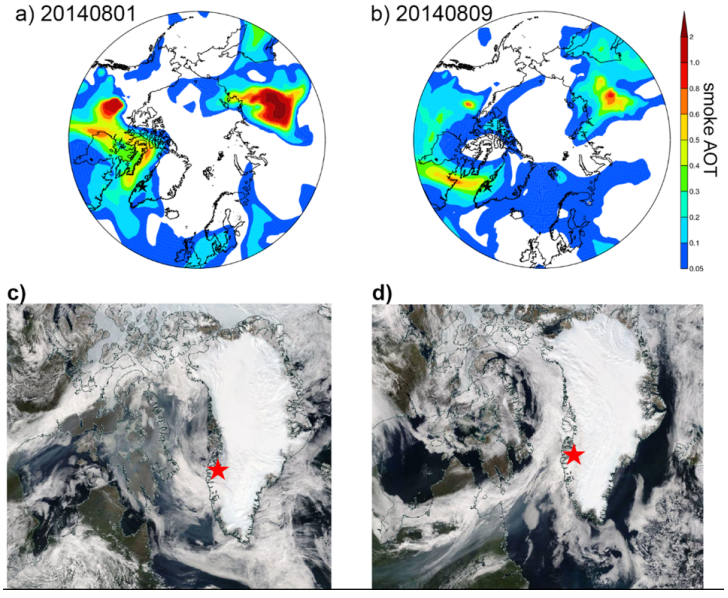

243

244 **Figure 4:** Biomass burning smoke transport reaching the GrIS from the west based NAAPS-RA
245 daily-mean smoke AOD and MODIS TERRA true color imageries for **A and C)** Aug. 1, 2014
246 and **B and D)** Aug. 9, 2014. The sampling location is marked with a black star in the NAAPS-
247 RA plots (A and B), and red stars in the MODIS imageries (C and D).

248 According to NAAPS model output, the deposition flux of smoke (Table 1 and Fig. 5)
249 onto the ice surface of the dark zone during our model study period, April 1st – August 30th, was
250 25.6 mg/m^2/day and 85% came from wet deposition. April 1st to August 30th was chosen based
251 on the primary Northern Hemisphere wildfire season and smoke transport to the Arctic (Xian et
252 al., 2022b). 68% of this smoke (17.3 mg/m^2/day) was deposited during our sample collection
253 period from June 27th to August 11th. Prior to the first sample collected on June 27th, 10% of the
254 total smoke flux (2.6 mg/m^2/day) was deposited from April 1st to June 26th. After the last sample
255 was collected on August 11th, 5.8 mg/m^2/day of smoke was deposited between August 12th and
256 30th.

https://doi.org/10.5194/tc-2022-258
Preprint. Discussion started: 22 February 2023

257 We evaluate the NAAPS-RA deposition flux based on the rBC concentration observed in
258 fresh snow, which was 3 µg-rBC/L-H_2O. The NAAPS model assumes 7% of smoke is BC. The
259 snow event that preceded the fresh snow sample collection, had a modeled precipitation rate of
260 10 mm/day or 10 L m^2. The modeled smoke deposition flux is 3000 µg/m^2/day or 300 µg/L. At
261 7% BC of total smoke, that leaves us with 21 µg-BC/L-H_2O. Therefore, the model appears to be
262 off by roughly a factor of 7 for this one snow sample. If we assume the snow water equivalent is
263 10%, then the rBC-snow concentration (i.e., the concentration of rBC in the fresh wet snow
264 being deposited) would be 2.1 µg-rBC/L-H_2O. Continued work is in progress to evaluate the
265 model across a larger sample size of rBC ground observations across the Arctic.
266 Two case studies of interest arise in the modelled total NAAPs smoke flux when
267 comparing wet and dry deposition. The first one is a large wet deposition flux and the second is a
268 considerable dry deposition flux. The first wet deposition flux ocurred between June 27th and 28th
269 (day of year 178 and 179), during a snow event (Fig. 5). Here we see the largest increase in the
270 total deposition flux of smoke over the study period at 5.0 mg/m^3/day in just over 24 hours.
271 99.8% of this comes from wet deposition. When we compare these model findings to the
272 observational rBC data in the surface hoar and snow, we see the rBC concentration in fresh
273 snow, 3 µg-rBC/L-H_2O, is high compared to pristine fresh snow previously found in Svalbard, 1
274 µg-rBC/L-H_2O (Khan et al., 2017). The average rBC concentration across the light, medium and
275 dark patches is also relatively high for a non-human impacted site in the polar regions (Cordero
276 et al., 2022). A previous study of black carbon in supra-glacial melt from the same GRIS site
277 previously confirmed the dissolved BC molecular signature was indicative of wildfire smoke that
278 likely came from Northern Canada and Alaska (Khan et al., 2017). Between July 22nd and
279 August 2nd, the model again shows a large proportion of the total deposition flux coming from

https://doi.org/10.5194/tc-2022-258
Preprint. Discussion started: 22 February 2023

wet deposition, 77% of the 3.2 mg/m^2/day. Similarly, from August 3rd to 11th, 86% of the 3.1 mg/m^3/day smoke deposition flux was from wet deposition. Again, this follows an increase in the total precipitation (Fig. 5).

However, a dry deposition case arises on July 21st, 2014. Here the NAAPs model does not produce a large total smoke deposition flux, but the rBC concentrations are still relatively high. Since the previous sampling event on June 28th, the model produces 0.2 mg/m^3/day total deposition flux, where only 16% comes from wet deposition. The majority, 84%, is from dry smoke deposition. This finding is also supported by the fact that there was little precipitation during this time based on the NAAPs modeled meteorology (Fig. 5), but it is also important to note that snow aging could also play a role in aggregation of BC particles. The decrease observed in the surface hoar rBC concentrations in the August 11th samples may suggest there was a process that removed the particles from the surface hoar, such as flushing or redistribution by supra-glacial melt, or uncontaminated fresh snow deposition which could dilute the concentrations. Further investigation into this process is warranted.

https://doi.org/10.5194/tc-2022-258
Preprint. Discussion started: 22 February 2023

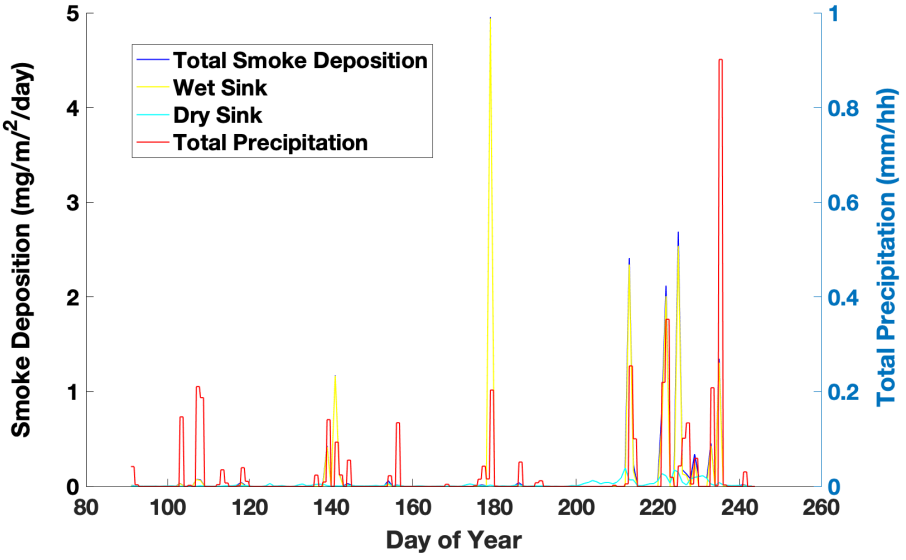

294

295 **Figure 5**: Biomass burning derived smoke deposition flux and total precipitation produced by
296 the NAAPS model. The total deposition flux is separated as wet and dry deposition. The total
297 smoke deposition closely follows the wet deposition line.

298

299 **4 Conclusion**

300 Here we present (to the author's knowledge) the first rBC size distributions from fresh snow
301 and surface hoar in the bare ice region of the GrIS, coupled with their concentrations. An initial
302 rBC size distribution in a fresh snow sample from the GrIS shows pronounced bimodality and
303 very large particles with the second peak almost 2 µm. These initial rBC size distributions from
304 surface hoar in the bare ice dark zone of the Greenland Ice Sheet are smaller than the fresh snow,
305 but still much larger than observations of atmospheric rBC. There appears to be a shift in the
306 modal peak of rBC particle size in light patches over the duration of the season from ~ 0.3 µm to
307 ~1.4 µm, further suggesting aggregation of particles in the bare-ice region. NAAPS-AOD and

https://doi.org/10.5194/tc-2022-258
Preprint. Discussion started: 22 February 2023

surface concentration data suggest that rBC surface hoar concentrations in the bare ice zone reflect atmospheric conditions momentarily, before possibly being reset by supra-glacial melt.

Additionally, we demonstrate preliminary verification of BC deposition from the NAAPs-RA with *in-situ* observations. rBC measurements in dark patches from late June to early August 2014 reveal an increase just after the smoke event. These elevated concentrations are closer to previously reported values in vertical snow and ice-core layers (e.g., Doherty et al., 2010 and Polashenski et al., 2013). The overall higher concentrations of rBC in visibly darker patches, where higher concentrations of ice algae were observed (Stibal et al., 2007), suggest potential bio flocculation with ice algae and mineral dust. However, NAAPS model results also indicate the increase is likely related to accumulation of deposition of wildfire-derived smoke, especially during episodically, such as the smoke event in early August, which brought smoke from the western Northern Hemisphere. Based on NAAPS deposition model and corroborated by rBC observations, wet deposition appears to be the largest source of rBC to the surface. For example, our fresh snow sample was measured at 3 µg-rBC/L-H_2O, while the model, off by a factor of 7, produced 21 µg-rBC/L-H_2O. These preliminary results suggest global aerosol models may be overestimating BC deposition; however, further investigation is warranted. These data provide utility in understanding the seasonal evolution of impurities, which are needed to constrain modeling of ice-albedo feedbacks in the bare-ice zone of the GRIS.

Author Contributions

ALK and JS analyzed the rBC samples. PX ran the NAAPs model and provided output data. ALK wrote the manuscript and PX and JS edited and contributed text. The samples were collected by ALK and the Dark Snow Project.

https://doi.org/10.5194/tc-2022-258
Preprint. Discussion started: 22 February 2023

Acknowledgements

The authors thank the Dark Snow Project for field support and additional sample collection, specifically, M. Stibal, J. Box and K. Cameron and N. Molotch.

Competing Interests. There are no conflicts of interest.

References

Baumgardner, D., Popovicheva, O., Allan, J., Bernardoni, V., Cao, J., Cavalli, F., et al. (2012). Soot reference materials for instrument calibration and intercomparisons : a workshop summary with recommendations. 1869–1887. doi:10.5194/amt-5-1869-2012.

Bond, T. C., Doherty, S. J., Fahey, D. W., Forster, P. M., Berntsen, T., DeAngelo, B. J., et al. (2013). Bounding the role of black carbon in the climate system: A scientific assessment. *J. Geophys. Res. Atmos.* 118, 5380–5552. doi:10.1002/jgrd.50171.

Cordero, R. R., Sepúlveda, E., Feron, S., Damiani, A., Fernandoy, F., Neshyba, S., ... & Casassa, G. (2022). Black carbon footprint of human presence in Antarctica. *Nature communications*, *13*(1), 1-11.

Doherty, S. J., Grenfell, T. C., Forsström, S., Hegg, D. L., Brandt, R. E., and Warren, S. G. (2013). Observed vertical redistribution of black carbon and other insoluble light-absorbing particles in melting snow. *J. Geophys. Res. Atmos.* 118, 5553–5569. doi:10.1002/jgrd.50235.

Doherty, S. J., Warren, S. G., Grenfell, T. C., Clarke, a. D., and Brandt, R. E. (2010a). Light-absorbing impurities in Arctic snow. *Atmos. Chem. Phys.* 10, 11647–11680. doi:10.5194/acp-10-11647-2010.

Doherty, S. J., Warren, S. G., Grenfell, T. C., Clarke, A. D., and Brandt, R. E. (2010b). and Physics Light-absorbing impurities in Arctic snow. 11647–11680. doi:10.5194/acp-10-11647-2010.

https://doi.org/10.5194/tc-2022-258
Preprint. Discussion started: 22 February 2023

357 Flanner, M. G., Zender, C. S., Randerson, J. T., and Rasch, P. J. (2007). Present-day climate
358 forcing and response from black carbon in snow. *J. Geophys. Res.* 112, D11202.
359 doi:10.1029/2006JD008003.
360 Greuell, W. (2000). Melt-water accumulation on the surface of the Greenland ice sheet: Effect on
361 albedo and mass balance. *Geogr. Ann. Ser. A Phys. Geogr.* 82, 489–498.
362 doi:10.1111/j.0435-3676.2000.00136.x.
363 Hanna, E., Huybrechts, P., Steffen, K., Cappelen, J., Huff, R., Shuman, C., et al. (2008).
364 Increased runoff from melt from the Greenland Ice Sheet: A response to global warming. *J.*
365 *Clim.* 21, 331–341. doi:10.1175/2007JCLI1964.1.
366 Katich, J. M., A. E. Perring, and J. P. Schwarz (2017), Optimized detection of particulates from
367 liquid samples in the aerosol phase: focus on black carbon, *Aeros. Sci. Technol.*,
368 doi:10.1080/02786826.2017.1280597
369 Keegan, K. M., Albert, M. R., Mcconnell, J. R., and Baker, I. (2014a). Climate change and forest
370 fires synergistically drive widespread melt events of the Greenland Ice Sheet. 1–4.
371 doi:10.1073/pnas.1405397111.
372 Keegan, K. M., Albert, M. R., McConnell, J. R., and Baker, I. (2014b). Climate change and
373 forest fires synergistically drive widespread melt events of the Greenland Ice Sheet. *Proc.*
374 *Natl. Acad. Sci. U. S. A.* 111. doi:10.1073/pnas.1405397111.
375 Khan, A. L., McMeeking, G. R., Schwarz, J. P., Xian, P., Welch, K. A., Berry Lyons, W., &
376 McKnight, D. M. (2018). Near-surface refractory black carbon observations in the
377 atmosphere and snow in the McMurdo dry valleys, Antarctica, and potential impacts of
378 Foehn winds. *Journal of Geophysical Research: Atmospheres*, *123*(5), 2877-2887.
379 Khan, A. L., H. Dierssen, J. P. Schwarz, C. Schmitt, A. Chlus, M. Hermanson, T. H. Painter,

and D. M. M. (2017). Journal of Geophysical Research : Atmospheres. *J. Geophys. Res. Atmos.*, 1–12. doi:10.1002/2016JD025757.

Khan, A.L., Wagner, S., Jaffe, R., Xian P. , Williams M., and Armstrong, R., and McKnight, D. (2017). Geophysical Research Letters. *Geophys. Res. Lett.*, 1–9. doi:10.1002/2017GL073485.

Lim, S., Faïn, X., Zanatta, M., Cozic, J., Jaffrezo, J.-L., Ginot, P., et al. (2014). Refractory black carbon mass concentrations in snow and ice: method evaluation and inter-comparison with elemental carbon measurement. *Atmos. Meas. Tech.* 7, 3549–3589. doi:10.5194/amtd-7-3549-2014.

Markowicz, K. M., et al. (2016), Impact of North American intense fires on aerosol optical properties measured over the European Arctic in July 2015, J. Geophys. Res. Atmos., 121, 14,487–14,512, doi:10.1002/2016JD025310.

Markowicz, K.M., Lisok, J., Xian, P., Simulation of long-term direct aerosol radiative forcing over the arctic within the framework of the iAREA project, Atmospheric Environment (2021), doi: https://doi.org/10.1016/j.atmosenv.2020.117882.

McConnell, J. R., Edwards, R., Kok, G. L., Flanner, M. G., Zender, C. S., Saltzman, E. S., et al. (2007a). 20th-century industrial black carbon emissions altered Arctic climate forcing. *Science (80-.).* 317, 1381–4. doi:10.1126/science.1144856.

McConnell, J. R., Edwards, R., Kok, G. L., Flanner, M. G., Zender, C. S., Saltzman, E. S., et al. (2007b). 20th-Century Industrial Black Carbon Emissions Altered Arctic Climate Forcing. *Science (80-.).* 317, 1381 LP – 1384. doi:10.1126/science.1144856.

Mori, T., Goto-Azuma, K., Kondo, Y., Ogawa-Tsukagawa, Y., Miura, K., Hirabayashi, M., et al. (2019). Black Carbon and Inorganic Aerosols in Arctic Snowpack. *J. Geophys. Res. Atmos.*,

403 2019JD030623. doi:10.1029/2019JD030623.

404 Polashenski, C. M., Dibb, J. E., Flanner, M. G., Chen, J. Y., Courville, Z. R., Lai, A. M., et al.
405 (2015a). Neither dust nor black carbon causing apparent albedo decline in Greenland's dry
406 snow zone: Implications for MODIS C5 surface reflectance. 9319–9327.
407 doi:10.1002/2015GL065912.Received.

408 Polashenski, C. M., Dibb, J. E., Flanner, M. G., Chen, J. Y., Courville, Z. R., Lai, A. M., et al.
409 (2015b). Neither dust nor black carbon causing apparent albedo decline in Greenland's dry
410 snow zone: Implications for MODIS C5 surface reflectance. *Geophys. Res. Lett.* 42.
411 doi:10.1002/2015GL065912.

412 Ranjbar, K., O'Neill, N. T., Lutsch, E., McCullough, E. M., AboEl-Fetouh, Y., Xian, P., et al.
413 (2019). Extreme smoke event over the high Arctic. *Atmos. Environ.* 218, 117002.
414 doi:https://doi.org/10.1016/j.atmosenv.2019.117002.

415 Reid, J. S., Koppmann, R., Eck, T. F., and Eleuterio, D. P.: A review of biomass burning
416 emissions part II: intensive physical properties of biomass burning particles, Atmos. Chem.
417 Phys., 5, 799–825, https://doi.org/10.5194/acp-5-799-2005, 2005.

418 Ryan, J. C., Hubbard, A., Stibal, M., Irvine-Fynn, T. D., Cook, J., Smith, L. C., et al. (2018).
419 Dark zone of the Greenland Ice Sheet controlled by distributed biologically-active
420 impurities. *Nat. Commun.* 9, 1–10. doi:10.1038/s41467-018-03353-2.

421 Ryan, J. C., Smith, L. C., Van As, D., Cooley, S. W., Cooper, M. G., Pitcher, L. H., et al. (2019).
422 Greenland Ice Sheet surface melt amplified by snowline migration and bare ice exposure.
423 *Sci. Adv.* 5, 1–11. doi:10.1126/sciadv.aav3738.

424 Schwarz, J. P., Doherty, S. J., Li, F., Ruggiero, S. T., Tanner, C. E., Perring, a. E., et al. (2012).
425 Assessing recent measurement techniques for quantifying black carbon concentration in

https://doi.org/10.5194/tc-2022-258
Preprint. Discussion started: 22 February 2023

426 snow. *Atmos. Meas. Tech. Discuss.* 5, 3771–3795. doi:10.5194/amtd-5-3771-2012.
427 Schwarz, J. P., Gao, R. S., Perring, a E., Spackman, J. R., and Fahey, D. W. (2013). Black
428 carbon aerosol size in snow. *Sci. Rep.* 3, 1356. doi:10.1038/srep01356.
429 Stibal, M., Box, J. E., Cameron, K. A., Langen, P. L., Yallop, M. L., M., H., R., Khan, A.L.,
430 Molotch, N. P., Chrismas, N.A.M., Quaglia, F.C., , Remias, D., Paul, C.J.P., Van den
431 Broeke, M., Ryan, J.,, Hubbard, A.,, Tranter, M., van As, D., and and Ahlstrøm, A. (2017).
432 Algae Drive Enhanced Darkening of Bare Ice on the Greenland Ice Sheet. *Geophys. Res.*
433 *Lett.*, 463–471. doi:10.1002/2017GL075958.
434 Stibal, M., Elster, J., Šabacká, M., and Kaštovská, K. (2007). Seasonal and diel changes in
435 photosynthetic activity of the snow alga Chlamydomonas nivalis (Chlorophyceae) from
436 Svalbard determined by pulse amplitude modulation fluorometry. *FEMS Microbiol. Ecol.*
437 59, 265–273. doi:10.1111/j.1574-6941.2006.00264.x.
438 Tedesco, M., Doherty, S., Fettweis, X., Alexander, P., Jeyaratnam, J., Noble, E., et al. (2016).
439 The darkening of the Greenland ice sheet: trends, drivers and projections
440 (1981–2100). *Cryosph.* 9, 5595–5645. doi:10.5194/tcd-9-5595-2015.
441 Wendl, I. a., Menking, J. a., Färber, R., Gysel, M., Kaspari, S. D., Laborde, M. J. G., et al.
442 (2014). Optimized method for black carbon analysis in ice and snow using the Single
443 Particle Soot Photometer. *Atmos. Meas. Tech.* 7, 3075–3111. doi:10.5194/amtd-7-3075-
444 2014.
445 Wientjes, I. G. M., Van De Wal, R. S. W., Reichart, G. J., Sluijs, A., and Oerlemans, J. (2011).
446 Dust from the dark region in the western ablation zone of the Greenland ice sheet.
447 *Cryosphere* 5, 589–601. doi:10.5194/tc-5-589-2011.
448

https://doi.org/10.5194/tc-2022-258
Preprint. Discussion started: 22 February 2023

449 Xian, P., Zhang, J., O'Neill, N. T., Toth, T. D., Sorenson, B., Colarco, P. R., Kipling, Z., Hyer, E.
450 J., Campbell, J. R., Reid, J. S., and Ranjbar, K.: Arctic spring and summertime aerosol
451 optical depth baseline from long-term observations and model reanalyses – Part 1:
452 Climatology and trend, Atmos. Chem. Phys., 22, 9915–9947, https://doi.org/10.5194/acp-
453 22-9915-2022, 2022.
454 Xian, P., Zhang, J., O'Neill, N. T., Reid, J. S., Toth, T. D., Sorenson, B., Hyer, E. J., Campbell, J.
455 R., and Ranjbar, K.: Arctic spring and summertime aerosol optical depth baseline from
456 long-term observations and model reanalyses – Part 2: Statistics of extreme AOD events,
457 and implications for the impact of regional biomass burning processes, Atmos. Chem.
458 Phys., 22, 9949–9967, https://doi.org/10.5194/acp-22-9949-2022, 2022.
459